Chemorepulsion from the Quorum Signal Autoinducer-2 Promotes *Helicobacter pylori* Biofilm Dispersal

Jeneva K. Anderson,[a] Julie Y. Huang,[b] Christopher Wreden,[a] Emily Goers Sweeney,[a] John Goers,[c] S. James Remington,[d] Karen Guillemin[a]

Institute of Molecular Biology, University of Oregon, Eugene, Oregon, USA[a]; Department of Microbiology and Immunology, Stanford University School of Medicine, Stanford, California, USA[b]; Department of Chemistry, California Polytechnic State University, San Luis Obispo, California, USA[c]; Department of Physics, University of Oregon, Eugene, Oregon, USA[d]

ABSTRACT The gastric pathogen *Helicobacter pylori* forms biofilms on abiotic and biotic surfaces. We have shown previously that *H. pylori* perceives the quorum signal autoinducer-2 (AI-2) as a chemorepellent. We report here that *H. pylori* chemorepulsion from endogenous AI-2 influences the proportions and spatial organization of cells within biofilms. Strains that fail to produce AI-2 ($\Delta luxS$ strains) or are defective for chemotaxis ($\Delta cheA$ strains) formed more spatially homogenous biofilms with a greater proportion of adherent versus planktonic cells than wild-type biofilms. Reciprocally, a strain that overproduced AI-2 ($luxS^{OP}$) formed biofilms with proportionally fewer adherent cells. Along with the known AI-2 chemoreceptor, TlpB, we identified AibA and AibB, two novel periplasmic binding proteins that are required for the AI-2 chemorepulsion response. Disruptions in any of the proteins required for AI-2 chemotaxis recapitulated the biofilm adherence and spatial organization phenotype of the $\Delta luxS$ mutant. Furthermore, exogenous administration of AI-2 was sufficient to decrease the proportion of adherent cells in biofilms and promote dispersal of cells from biofilms in a chemotaxis-dependent manner. Finally, we found that disruption of AI-2 production or AI-2 chemotaxis resulted in increased clustering of cells in microcolonies on cultured epithelial cells. We conclude that chemotaxis from AI-2 is a determinant of *H. pylori* biofilm spatial organization and dispersal.

IMPORTANCE Bacterial biofilms are ubiquitous in nature, but the mechanisms governing their assembly and spatial organization are not fully understood. Bacterial communication through quorum sensing has been shown to influence biofilm growth through the regulation of biofilm genes. Our study revealed a new role for quorum sensing in biofilms through rapid chemotactic responses to quorum signals. Specifically, we studied how chemorepulsion of *Helicobacter pylori* from the universal quorum signal autoinducer-2 (AI-2) shapes the spatial organization of its biofilms. We demonstrate that the chemorepulsive response of *H. pylori* to AI-2 is necessary to promote its dispersal from biofilms grown on both abiotic and biotic surfaces and is sufficient to promote dispersal in a chemotaxis-dependent manner. This work has broad implications for understanding the mechanisms by which endogenously produced microbial compounds shape the assembly and spatial organization of microbial communities in their environments.

Address correspondence to Karen Guillemin, guillemin@molbio.uoregon.edu.

In nature, bacteria often reside within multispecies aggregate communities called biofilms that serve to protect the cells from environmental challenges (1–5). Within these aggregated communities, bacterial cells secrete molecules that allow the biofilm to grow at environmental interfaces and attach to other cells and biotic or abiotic surfaces (6, 7). The persistence of biofilms on biotic surfaces, such as the lung epithelia of cystic fibrosis patients, or on abiotic surfaces, such as medical implants, poses serious human health risks (4, 8–10). Despite the medical importance of biofilm growth, many unanswered questions remain about the mechanisms that drive biofilm dynamics.

Biofilm formation is initiated by attachment of single cells to a surface, and these adherent cells grow into microcolonies as clonal populations. These microcolonies can further develop into mature biofilms that produce extracellular matrix molecules to maintain cellular aggregates with distinct organizations and structures (4). This process is dynamic, with continuous joining and separation of cells in response to changes in the environment (6, 9). The biofilm life cycle involves cellular processes that occur over different time scales and that require long-term cell fate commitments as well as a need for bacterial cells to respond quickly to changes in the environment.

In many bacterial species, biofilm formation is influenced by quorum sensing, a mechanism bacteria use to coordinate their behavior (11–13). Quorum sensing involves the production of small molecules that are secreted into the environment and sensed by other bacterial cells in a population density-dependent manner (11). Often, the recipient bacteria respond to quorum-sensing molecules by inducing changes in expression of genes, such as those involved in long-term commitment to a sessile or plank-

tonic lifestyle (11). For example, quorum-sensing-regulated genes are involved in the production of exopolysaccharides, lipids, nucleic acids, and proteases that are required to build the biofilm matrix (14–17).

Quorum sensing can also elicit more immediate changes in bacterial behaviors by directing cellular motility through chemotactic responses. For example, in the predatory bacterial species *Myxococcus xanthus*, a secreted small molecule called A-factor alters motility and promotes aggregation and the initiation of fruiting body biofilm formation (18–20). Importantly for this study, the quorum-sensing molecule autoinducer-2 (AI-2), an interspecies quorum-sensing molecule produced by the conserved metabolic enzyme LuxS, elicits chemotactic responses in multiple bacteria (21, 22). In the enteric commensal *Escherichia coli*, AI-2 elicits an attractant response (21), whereas in the gastric pathogen *Helicobacter pylori*, AI-2 is sensed as a repellant (22). In this study, we addressed how these rapid responses to quorum-sensing molecules influence spatial distributions of cells within a biofilm community.

To explore this issue, we studied the role of AI-2 chemotactic responses in *H. pylori* biofilm formation on abiotic and biotic surfaces. Previous work has shown that *H. pylori* bacteria form microcolonies and biofilms both *in vitro* on cultured epithelial cells and *in vivo*, as revealed in human stomach biopsy specimens (23–30). Additionally, *H. pylori* may form heterotropic biofilms in water reservoirs (31–33). Mature *H. pylori* biofilms have been shown to contain extracellular DNA (eDNA) as well as an exopolysaccharide matrix (33, 34) similar to those made by other biofilm-forming species. Biofilm formation is thought to be functionally important for *H. pylori* in providing a natural reservoir in drinking water systems and providing protection from antibiotics (33).

The role of LuxS in *H. pylori* biofilm formation has been studied previously (24, 33, 35). Relevant to our study, Cole et al. showed that a *luxS*-deficient *H. pylori* mutant exhibited increased levels of adherence to glass frit relative to a wild-type (WT) strain (24). Here we replicated this finding and tested whether it was due to loss of an endogenously produced chemorepulsive cue. We investigated the impacts of AI-2 production and sensing during early and late stages of biofilm growth and show that AI-2 chemotaxis is an important modulator of the equilibrium between planktonic and biofilm cells and of the spatial distribution of cells within the biofilm. We defined the molecular basis for AI-2 chemoreception in *H. pylori*, identifying two new AI-2 periplasmic binding proteins (PBPs) that are essential for this process. Additionally, we demonstrated that disruption of AI-2 production or AI-2 chemotaxis results in an increase in the size of *H. pylori* microcolonies on cultured epithelial cells. Our work supports the idea of a novel mechanism whereby rapid chemotactic responses of individual cells to quorum-sensing molecules contribute to the long-term spatial organization and aggregation properties of biofilms.

RESULTS

AI-2 production and chemotaxis influence biofilm organization. To investigate the importance of AI-2 chemorepulsion for *H. pylori* biology, we examined *H. pylori* biofilm organization as a function of AI-2 production. We spotted liquid cultures of G27 wild-type (WT) and isogenic Δ*luxS* strains of *H. pylori* onto sterile glass slides, which were cultured under static, humidifying, and high-CO_2 conditions for 5 days (the minimal time required for sufficient biofilm mass to accumulate for microscopic visualization). The biofilms that formed at the air-liquid interface were fixed, stained with the DNA dye 4′,6-diamidino-2-phenylindole (DAPI), and imaged using fluorescence microscopy (Fig. 1A to E). Upon visualization, it was immediately apparent that the wild-type and Δ*luxS* cells differed in their spatial distributions in biofilms. WT cells formed discrete multicellular aggregates, whereas the Δ*luxS* cells formed a homogeneous mat of cells (Fig. 1A and B). Genetic complementation of *luxS* (*luxS**) was able to restore biofilm organization to the WT pattern (Fig. 1C). This result suggests that LuxS is required for normal multicellular organization within biofilms. We next wanted to test if increasing endogenous AI-2 production would alter the cellular organization in biofilms. We engineered a strain with an extra chromosomal copy of the *luxS* gene (*luxS^{OP}* [overproducer]) expressed from the native *luxS* promoter and confirmed that this strain grew with kinetics similar to WT kinetics (see Fig. S1A in the supplemental material) and produced more AI-2 (see Fig. S1B). Upon biofilm visualization, we observed that the cellular organization of the *luxS^{OP}* strain was similar to that of the WT strain (Fig. 1D).

Fractal dimension and lacunarity have been used to quantify differences in the spatial organization of biofilms (36, 37). Fractal dimension data quantify the complexity of the image, while lacunarity measures the extent of discontinuities or inhomogeneity of the image (36). We used FracLac (an ImageJ plugin) to calculate the fractal dimension and the lacunarity score for epifluorescence images of biofilms for which threshold values were calculated (i.e., thresholded) using contrast-limited adaptive histogram equalization (see Fig. S2 in the supplemental material). Although we observed no differences in comparisons of the fractal dimension data from any of the strains (data not shown), we did observe differences in lacunarity scores that correlate with perceived differences in the images (Fig. 1F). The Δ*luxS* strain had a significantly lower lacunarity score than the WT strain, indicating more homogeneity. Reciprocally, the lacunarity score was significantly higher for the *luxS^{OP}* strain than for the WT strain, indicating more spatial inhomogeneity. We conclude that the spatial organization of cells in biofilms is dependent on levels of AI-2 production.

The overall biofilm structure is the result of dynamic interactions of cells transitioning between sessile and planktonic states. We wished to quantify the fraction of the population in each of these states. To do so, we grew *H. pylori* cultures under static, high-CO_2 conditions in wells filled with glass frit to provide abundant surfaces for biofilm formation (Fig. 1G; adapted from reference 24). We used crystal violet staining to quantify the populations of adherent and planktonic cells, and we report the percentages of adherent cells in the total cell population as the percentages of biofilm cells. In time course analyses of the biofilms, we observed no significant changes between 2 and 6 days postinoculation in the proportions of adherent and planktonic cells or in the total numbers of cells in the system (see Fig. S3A and B in the supplemental material). All subsequent analyses of biofilms grown on glass frit were performed at 2 days postinoculation. In comparisons of the percentages of biofilm cells of the WT and *luxS* derivatives, we observed that the Δ*luxS* strain had a significantly higher proportion of adherent cells than the WT and the *luxS** strains (Fig. 1H). We verified that, under the conditions that produced differential biofilm formation results (see Fig. 3C), AI-2 was detected at comparable levels in the media of the WT and
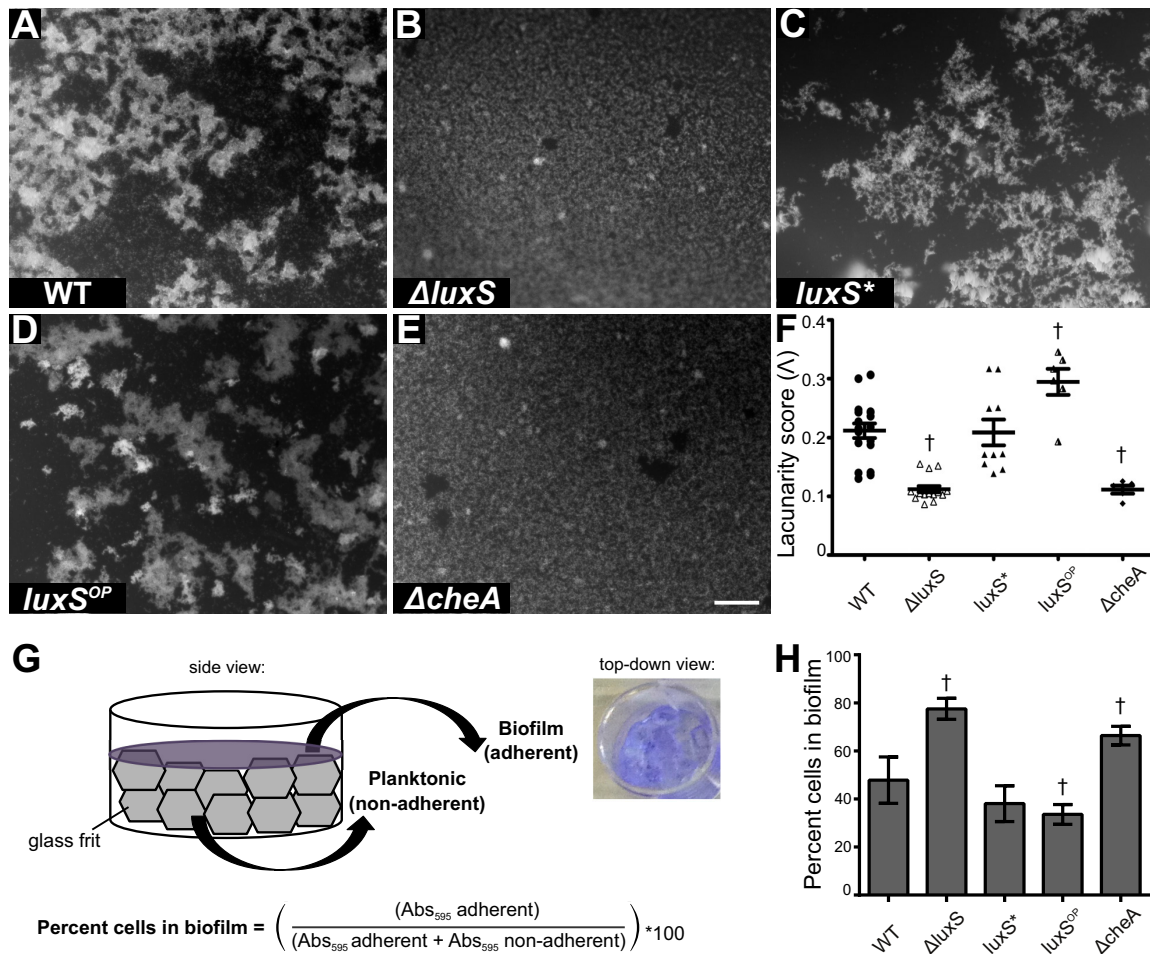
FIG 1 Endogenous AI-2 production and chemotaxis alter biofilm organization. (A to E) Epifluorescence images of wild-type and mutant G27 *H. pylori* biofilms grown on glass slides for 5 days. Cells were fixed and stained with DAPI (white). Bar, 100 μm. (F) Lacunarity scores for biofilm images. Each dot represents the lacunarity score for a single epifluorescence biofilm image postthresholding, with corresponding means and standard deviations. (G) Schematic of glass frit biofilm assay with crystal violet analysis and examples of percentages of cells in the biofilm calculation. (H) Effect of AI-2 production and chemotaxis on adherence of cells in biofilms on glass frit after 2 days, as quantified by the crystal violet assay. Error bars represent standard errors of the means of the results of a minimum of three experiments for each strain. Daggers indicate a significant ($P < 0.05$) difference from the wild-type results determined using Student's *t* test (F) or one-way analysis of variance (H).

luxS* cultures and at low levels in the Δ*luxS* culture (see Fig. 3E). We also characterized the biofilm growth of the *luxS*^OP^ strain, which produces more AI-2 than the WT strain (Fig. S1), and observed a modest but significant reduction in the proportion of adherent cells compared to the results seen with wild-type biofilms (Fig. 1H). Together, these results suggest that normal biofilm formation and organization of *H. pylori* G27 are modulated by levels of endogenously produced AI-2.

We hypothesized that the differences in biofilm organization that we observed were due to chemorepulsion from endogenously produced AI-2. To test this, we investigated the biofilm formation of a chemotaxis-deficient strain, strain Δ*cheA*, which lacks the CheA signal transduction protein required for actuating chemotactic responses. The cellular organization of Δ*cheA* biofilms resembled those observed with the Δ*luxS* strain, with uniform films of cells (Fig. 1E) and a lacunarity score significantly lower than the WT strain score (Fig. 1F). Consistent with this observation, the Δ*cheA* mutant displayed increased proportional adherence compared to the WT strain (Fig. 1H). This indicates that chemotaxis

plays an important role in dictating cellular organization and adherence within *H. pylori* biofilms.

Chemotactic responses to AI-2 require two novel periplasmic AI-2 binding proteins. Because LuxS functions as both a quorum signal synthase and a metabolic enzyme (38), the biofilm defects of the Δ*luxS* could be due to other cellular phenotypes in addition to loss of AI-2 chemorepulsion. To better test our hypothesis that biofilm organization is modulated by AI-2-induced chemorepulsion, we sought to identify the proteins specifically involved in AI-2 chemorepulsion in *H. pylori*. In *E. coli*, AI-2 chemotaxis requires the chemoreceptor Tsr and the periplasmic binding protein LsrB (21). We have previously shown that in *H. pylori*, AI-2 chemorepulsion requires the chemoreceptor TlpB (22); however, there is no homolog of LsrB in *H. pylori* as determined by BLAST protein sequence alignment (39). Chemoreceptors signal via direct ligand binding or through interactions with ligand binding proteins that transduce signals to the chemoreceptor (40). Given the lack of a LsrB homolog in *H. pylori*, we assessed whether TlpB could bind AI-2 directly. We adapted an *in vitro*
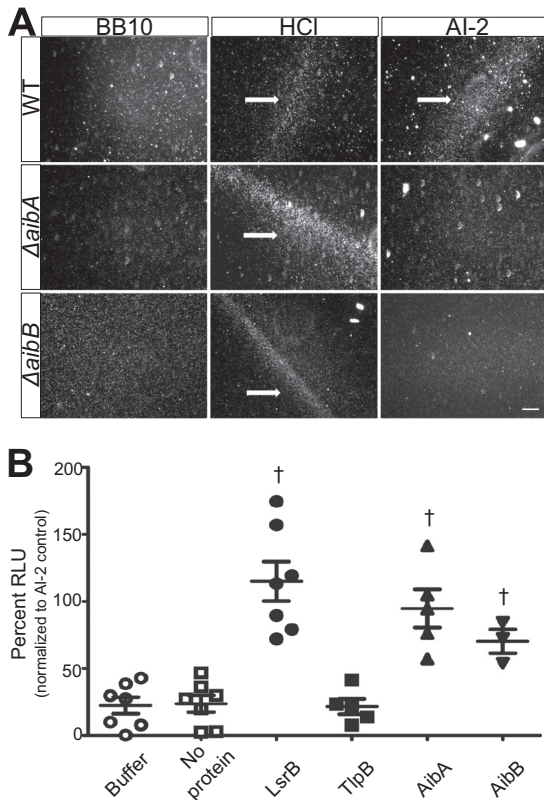
FIG 2 AI-2 chemotaxis requires two periplasmic binding proteins, AibA and AibB, that bind AI-2 independently. (A) Chemotaxis response of wild-type and ΔHPG27_277 (ΔaibA) and ΔHPG27_431 (ΔaibB) mutant *H. pylori* to brucella broth (BB10), 100 mM HCl, and 100 μM synthetic DPD (AI-2). Representative wet-mount images of bacterial cells (white dots) are shown. Formation of a barrier (marked by white arrows) indicates a chemotactic response. Bar, 200 μm. (B) *In vitro* AI-2 binding assay performed with purified proteins using a *V. harveyi* bioluminescence readout. Percentages of relative luminescence units (RLU) were normalized to an AI-2 positive control in each independent experiment. Error bars represent standard errors of the means of the results of comparisons of experimental data. Daggers indicate a significant ($P < 0.05$) difference from the buffer negative-control results determined using Student's *t* test.

AI-2 binding assay (41, 42) in which AI-2 was incubated with either the purified periplasmic portion of TlpB or, as a positive control, purified LsrB protein, which binds AI-2 with a dissociation constant (K_d) of 160 μM (43). To quantify AI-2 binding, proteins were purified away from unbound AI-2 and denatured to release bound AI-2, and the supernatant was used to stimulate *Vibrio harveyi* luminescence. As expected, the luminescence levels induced by the LsrB supernatant were high, indicating the presence of bound AI-2 (Fig. 2B). In contrast, the luminescence levels stimulated by TlpB were not above background levels. This suggests that TlpB does not bind AI-2 *in vitro* with high affinity and may require additional proteins.

We hypothesized that a periplasmic binding protein (PBP) in *H. pylori* performs a function similar to that performed by LsrB. We identified five hypothetical proteins in G27 that were homologous to other periplasmic transport and binding proteins: *H. pylori* G27_277 (HPG27_277), HPG27_431, HPG27_889, HPG27_1116, and HPG27_1197. We tested these potential candidates for their requirement in AI-2 chemorepulsion by making

nonpolar deletions of each PBP individually via allelic exchange and assessed the ability of these mutants to respond to AI-2. We tested the chemorepellant responses of these mutants to 100 μM AI-2 using a previously described barrier assay (22). In this assay, formation of a barrier of swimming cells away from the source of the chemical indicates a repellant response. We showed previously that ΔtlpB and ΔcheA mutants do not form barriers in response to AI-2 compared to WT strains (22). We discovered that two of the five PBP mutants, ΔHPG27_277 and ΔHPG27_431, also failed to form barriers in response to AI-2, although they still formed barriers in response to another known chemorepellant, HCl (Fig. 2A). These results suggest that these two putative PBPs are independently required for AI-2 chemotaxis. The other three PBP mutants remained responsive to AI-2 (see Fig. S4 in the supplemental material). Within the genome of strain G27, the HPG27_277 and HPG27_431 genes are located within operons involved in dipeptide transport and molybdate transport, respectively (see Fig. S5A and B); however, it is not uncommon for PBPs to have multiple transport and binding functions within the cell (40).

Using the *in vitro* AI-2 binding assay described above, we tested the ability of these two proteins to bind AI-2. For this assay, we constructed HPG27_277 and HPG27_431 variants lacking their hydrophobic periplasmic targeting sequences for ease of purification. We observed significant AI-2 binding capacity for both HPG27_277 and HPG27_431 proteins similar to that seen with the LsrB positive control (Fig. 2B). These results indicate that HPG27_277 and HPG27_431 bind AI-2 directly *in vitro* and independently of one another. Due to this identified function, we named HPG27_277 AibA and HPG27_431 AibB, for <u>AI</u>-2 <u>b</u>inding proteins A and B.

TlpB, AibA, and AibB are necessary for biofilm organization. To further test the hypothesis that AI-2 chemotaxis influences the spatial organization of cells within biofilms, we observed biofilms of strains lacking AI-2 chemoreception (strains ΔtlpB, ΔaibA, and ΔaibB and the double mutant ΔaibA ΔaibB) grown on glass slides, as previously described (Fig. 3A to G). We found that the cellular organization of all AI-2 chemotaxis-deficient strains (Fig. 3A, C, E, and G) recapitulated the biofilm structures of the ΔluxS-deficient and ΔcheA-deficient *H. pylori* strains. Consistent with this observation, the lacunarity scores for the biofilms of these strains were significantly lower than the WT score (Fig. 3H) and were similar to scores observed with the ΔluxS and ΔcheA strains (compare to Fig. 1F).

We also quantified the proportions of adherent and planktonic cells within 2-day biofilms of the ΔtlpB, ΔaibA, ΔaibB, and ΔaibA ΔaibB strains grown on glass frit. Under these growth conditions, the total numbers of cells within the cultures (adherent and planktonic) of all strains were similar (see Fig. S5C), but we found that the AI-2 chemotaxis-deficient strains had proportional adherence in biofilms that was significantly increased compared to that seen with the WT strain (Fig. 3I) and similar to that seen with the ΔluxS and ΔcheA strains (compare to Fig. 1H).

We next attempted to complement these biofilm defects in the AI-2 chemotaxis-deficient strains. Genetic complementation in *H. pylori* is limited by the precision with which genes can be expressed from heterologous loci. To complement TlpB, we made use of an engineered mutation (TlpB^D114N) (44) in the endogenous locus that we have shown disrupts acid sensing but not AI-2 chemorepulsion. We found that this variant of TlpB was able to
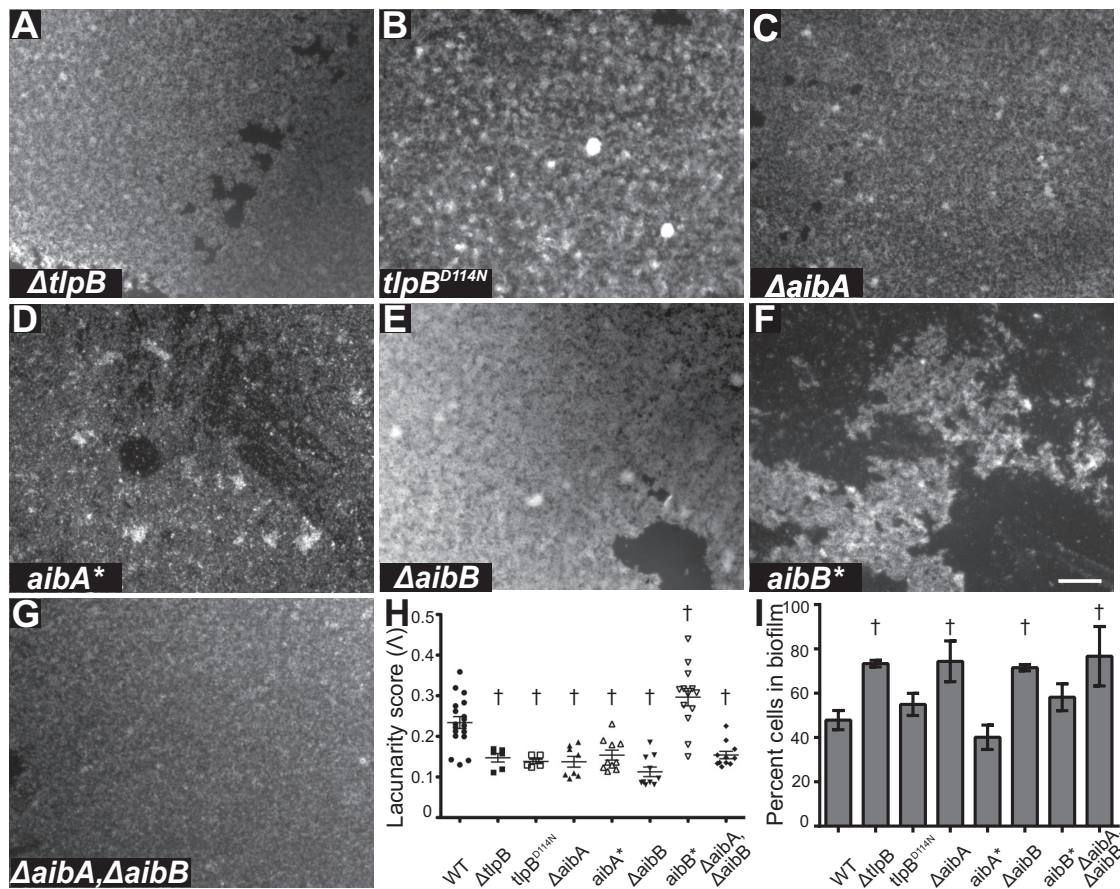
FIG 3 Chemorepulsion from AI-2 is necessary for biofilm organization. (A to G) Epifluorescence images of AI-2 chemotaxis-defective mutants and complemented-strain biofilms grown on glass slides for 5 days. Cells were fixed and stained with DAPI (white). (H) Lacunarity scores for biofilm images. Each point represents the lacunarity score for a single epifluorescence biofilm image postthresholding, with corresponding means and standard deviations. (I) Effect of AI-2 chemotaxis disruption on adherence of cells in biofilms on glass frit after 2 days, as quantified by the crystal violet assay. Error bars represent standard errors of the means of the results of a minimum of 3 experiments for each strain. Daggers indicate a significant ($P < 0.05$) difference from the wild-type results determined using Student's *t* test (H) or one-way analysis of variance (I).

restore a normal proportion of adhesion in the biofilm (Fig. 3I) but that it did not rescue the cellular organization phenotype (Fig. 3B) or the lacunarity of the biofilms (Fig. 3H). Complementation of *aibA* deficiency was achieved by inserting the wild-type *aibA* gene at the *rdx* locus (*aibA**). Due to *aibA* being part of a potential operon, we engineered the putative *aibB* promoter into the *rdx* locus to drive expression of *aibA*. As with TlpB, complementation of *aibA* did restore proportional adhesion in the biofilm (Fig. 3I) but was unable to rescue the ΔaibA mutant spatial organization (Fig. 3D and H). Complementation of ΔaibB was also achieved by restoration of the wild-type gene and putative promoter at the *rdx* locus (*aibB**). In this case, complementation restored the normal proportional adhesion (Fig. 3I) and was able to rescue the spatial organization of cells in the biofilm with respect to the WT spatial patterning (Fig. 3F), with a lacunarity score slightly higher than the WT score (Fig. 3H; P = 0.04 by Student's *t* test). We hypothesized that the partial rescue in lacunarity observed in the *aibA** and *tlpB*^{D114N} strains might have due to decreased expression compared to the WT level. To address this hypothesis, we used quantitative reverse transcription-PCR (qRT-PCR) to quantify the relative amounts of *aibA*, *aibB* and *tlpB* transcripts in the complemented strains compared to the WT amounts

(see Fig. S6 in the supplemental material). We observed that the levels of *aibB* in the *aibB** strain were roughly equivalent to the WT levels (see Fig. S6, WT$_{aibB}$ and *aibB**), and, indeed, we observed full rescue of biofilm phenotypes with this strain (Fig. 3F, H, and I). The levels of *aibA* in the *aibA** strain were approximately 60% of the levels of *aibA* in the WT strain (see Fig. S6, WT$_{aibA}$ and *aibA**). This may explain why we observed incomplete rescue of the spatial organization and lacunarity of *aibA** biofilms (Fig. 3D and H). We observed that the *tlpB*^{D114N} complement had levels of *tlpB* transcript similar to those seen with the WT strain (see Fig. S6, WT$_{tlpB}$ and *tlpB*^{D114N}), consistent with the WT levels of protein expression in this strain (44). However, this study also showed that the TlpB^{D114N} protein is less stable than the WT TlpB protein *in vitro*, which could explain the incomplete rescue of the *tlpB*^{D114N} biofilm spatial organization and lacunarity (Fig. 3B and H).

AI-2 is sufficient to alter biofilm organization during biofilm formation in a chemotaxis-dependent manner. Having demonstrated that AI-2 production and chemotaxis are necessary for normal biofilm formation, we next wanted to extend our findings by manipulating the system with exogenously added AI-2. To accomplish this, we added AI-2 at the time of inoculation of cells
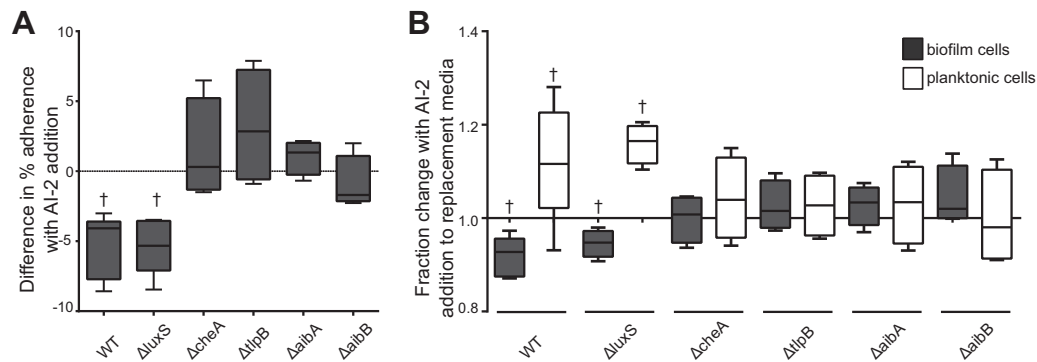
FIG 4 Chemorepulsion from AI-2 is sufficient to decrease adherence in biofilms. (A) Change in adherence of strains in biofilm with addition of exogenous AI-2 (37 nM) at the time of inoculation. Daggers indicate a significant ($P < 0.05$) difference from 0 (no change) determined using Student's t test. (B) Fraction changes in biofilm size (grey bars) and numbers of planktonic cells (white bars) measured 72 h after the initiation of the biofilms and 24 h after rinsing and exchange with fresh media containing 37 nM exogenous AI-2. Daggers indicate a significant ($P < 0.05$) difference from a value of 1 (no change) determined using Student's t test. Box plots show means and standard deviations of the results of a minimum of three experiments for each strain.

into wells containing glass frit and quantified the differences in the percentages of cells in the biofilm (Fig. 4A). We determined empirically that 37 nM AI-2, a concentration within the range produced endogenously by *H. pylori* (45), caused the greatest effect in these assays, and we used this concentration in all subsequent experiments. We found that exogenous AI-2 reduced the proportion of adhered WT *H. pylori* bacteria measured 2 days after initiation of biofilm formation and AI-2 addition. We also observed a significant reduction in adherence for the Δ*luxS* strain upon addition of AI-2. This is consistent with the fact that, although the *luxS*-deficient strain is unable to produce AI-2, it can still respond to exogenous AI-2 (45). We next performed this experiment with the AI-2 chemotaxis-deficient Δ*cheA*, Δ*tlpB*, Δ*aibA*, and Δ*aibB* strains. Consistent with the inability of these strains to sense AI-2, they exhibited no differences in the proportions of adherent cells in the presence or absence of exogenous AI-2. These results indicate that biofilm organizational patterning induced by AI-2 requires intact AI-2 sensing and that the presence of AI-2 is sufficient to decrease adherence in biofilms during the early stages of biofilm formation.

We next tested directly whether AI-2 chemotaxis acted to decrease adherence in biofilms by promoting dispersal from mature biofilms. We grew biofilms of the WT and Δ*luxS* strains for 48 h, gently removed the media containing planktonic cells, and replaced it with fresh media either with or without exogenous AI-2 (37 nM). At this time point, adherent cells were readily visible on the sides of the well and on the glass frit. After another 24-h incubation, we quantified the populations of planktonic and adherent cells. Because we removed planktonic cells from the wells at 48 h, we assumed that all cells entering the planktonic population after replacement of media were ones that had dispersed from the preexisting biofilm. We calculated the changes in the biofilm (adherent) populations between cultures treated with AI-2 and untreated controls and separately calculated the changes in the planktonic (nonadherent) populations of the two treatment groups (Fig. 4B). Both the WT and Δ*luxS* strains exhibited a decrease in their biofilm populations upon AI-2 addition, suggesting that the presence of AI-2 was sufficient to have triggered partial biofilm dispersal. Reciprocally, there was an increase in the numbers of the planktonic cells of these two strains upon addition of AI-2. To confirm the role of chemotaxis in AI-2-mediated biofilm

dispersal, we examined the response of the Δ*cheA*, Δ*tlpB*, Δ*aibA*, and Δ*aibB* mutant biofilms to AI-2 addition. We found no significant difference in the biofilm or the planktonic populations of any of these strains upon the addition of AI-2. These results indicate that AI-2 promotes dispersal of cells from preexisting biofilms by a chemotaxis-dependent mechanism.

Abolishing AI-2 production or AI-2 chemotaxis results in formation of larger microcolonies on cultured epithelial cells. We wanted to test whether this AI-2 chemotaxis response was relevant to the fitness of *H. pylori* on epithelial cells, where they experience a set of chemical signals different from those experienced on abiotic surfaces. To do this, we adapted a previously described microcolony assay (25) using polarized Madin-Darby canine kidney (MDCK) epithelial cells seeded onto a transwell filter. We used the G27MA strain, which had been adapted to grow well on MDCK cells (46), in contrast to the parental G27 strain, which does not grow well in this assay (data not shown). We infected MDCK monolayers with WT G27MA and isogenic Δ*luxS*, Δ*cheA*, Δ*cheW* (a mutant functionally similar to Δ*cheA*), Δ*tlpB*, Δ*aibA*, and Δ*aibB* strains to test if AI-2 production or chemotaxis influences the size of the microcolonies formed. The attached bacteria grew on the epithelial cells and formed aggregates or microcolonies. We hypothesized that, similarly to what we observed in the *in vitro* biofilm formation results, there would be increased dispersal of cells from microcolonies in an AI-2 chemotaxis-dependent manner.

To test this, we fixed and stained the infected transwells to visualize *H. pylori* cells and MDCK cell junctions (ZO-1) at 5 min postinfection (initial attachment) and at 3 days postinfection (Fig. 5A to C). To determine if all strains had equivalent levels of growth and attachment on the MDCK cells, we estimated the quantities of attached bacteria present on the cell layer at 5 min and 3 days postinfection. To do this, we quantified the average microcolony sizes of cells in at least 3 fields of triplicate transwells for each condition and used the size measurement of a single *H. pylori* cell (20 pixels) to estimate the number of *H. pylori* cells in the image. We then extrapolated this to estimate the number of attached *H. pylori* cells in the entire transwell (Fig. 5D). We observed that the WT, Δ*luxS*, and Δ*tlpB* strains had significantly increased numbers of attached bacteria from 5 min to 3 days postinfection. However, for the Δ*cheW*, Δ*cheA*, Δ*aibA*, and Δ*aibB*
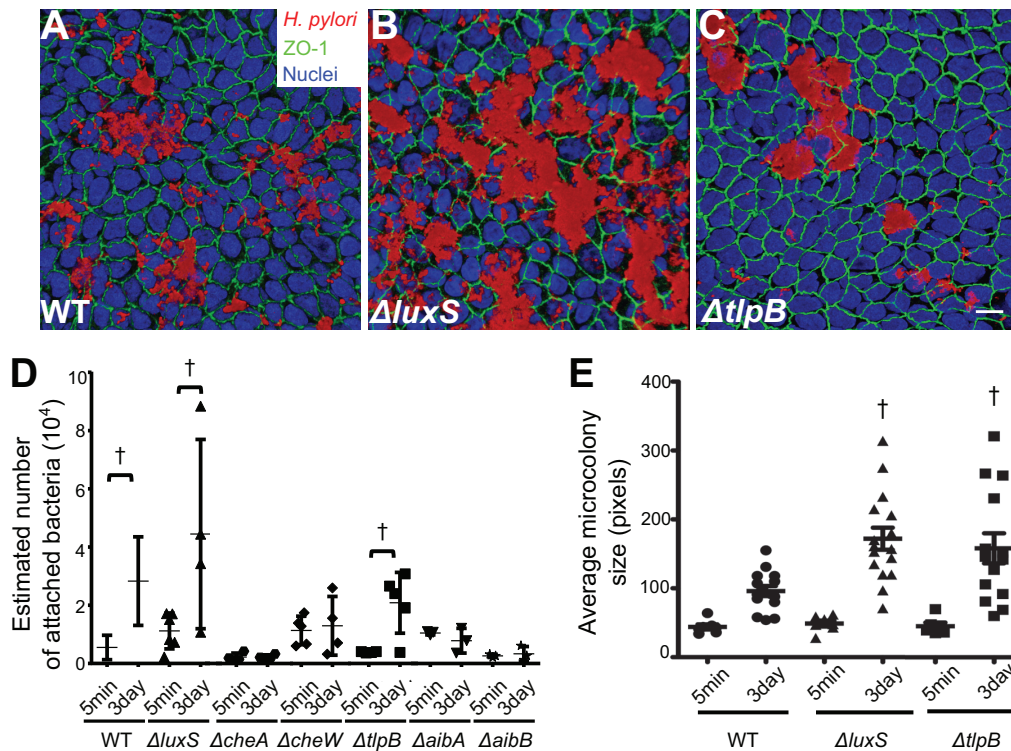
FIG 5 Disruption of either AI-2 production or AI-2 chemotaxis results in larger microcolonies on cultured epithelial cell monolayers. (A to C) Representative images of WT, Δ*luxS*, and Δ*tlpB* *H. pylori* microcolonies on polarized MDCK monolayers at 3 days postinfection. *H. pylori* cells are visualized in red, nuclei in blue, and cell junctions in green. Bar, 10 μm. (D) Estimated numbers of attached bacteria on the MDCK epithelial cell layer at 5 min and 3 days postinfection for all strains. Each point represents the estimated number of bacteria averaged over multiple images per transwell. Error bars represent standard errors of the means. Daggers represent significant increases in numbers of attached bacteria from 5 min to 3 days of attachment for each strain. (E) Plot of the surface area covered by contiguous clusters of bacterial cells (microcolonies) for each strain at 5 min (predominantly isolated single cells) and 3 days postinoculation. Each dot represents the average area (in pixels) of all the microcolonies in an image. Three images were taken per transwell, with three replicate transwells per experiment. Error bars represent standard errors of the means. Daggers represent significant ($P < 0.05$) increases of pixel sizes compared to the WT results through the use of one-way analysis of variance.

strains, we observed no significant increase in the numbers of attached bacteria over the course of the experiment. There are several possible explanations for this observation, including lack of growth on the MDCK cells, defects in attachment, or increased dispersal of cells from microcolonies. Given the ambiguity of the significance of the lack of growth of these strains in this assay, we did not evaluate them further.

For the WT, Δ*luxS*, and Δ*tlpB* strains that were able to grow on MDCK cell epithelia, we determined the average microcolony size at 5 min postinfection (see Fig. S7 in the supplemental material) and at 3 days postinfection (Fig. 5E). We found that the Δ*luxS* strain had a significant increase in microcolony size at 3 days postinfection compared to the WT strain, while there was no significant difference with respect to initial attachment (Fig. 5E). Thus, disruption *of luxS* resulted in an increase in the size of the adherent microcolonies, which is consistent with our observations of decreased dispersal of *luxS* cells in the *in vitro* biofilm assays (Fig. 1H). Also consistent with our predictions, we observed that the lack of *tlpB* resulted in microcolony sizes significantly larger than those seen with the WT strain and similar to those seen with the Δ*luxS* strain (Fig. 5E). Taken together, these results suggest that AI-2 chemorepulsion is important for promoting *H. pylori* dispersal from cell aggregates on epithelial cell surfaces.

DISCUSSION

For many bacterial species, quorum sensing has been well characterized to influence biofilm formation through the regulation of gene expression. Here we introduce a new role for quorum sensing in shaping biofilms on a much shorter time scale through chemotactic responses of cells to quorum signals. We provide evidence that *H. pylori* biofilm dispersal and cellular spatial organization are shaped by chemorepulsive responses to AI-2 in *H. pylori*.

***H. pylori* uses a novel AI-2 sensing mechanism.** Although many bacterial species produce and sense AI-2, mechanisms for AI-2 sensing are not strictly conserved among them. Prior to this work, two examples had been described for AI-2 sensing: one operating through the periplasmic LuxP binding partner of the LuxQ histidine kinase in *Vibrio* species and a second through the PBP LsrB in several phylogenetically distinct families, serving as both an AI-2 transport protein and a binding partner for the Tsr chemoreceptor (41, 47, 48). In this study, we investigated the molecular basis for AI-2 chemoreception in *H. pylori* and discovered two PBPs, AibA and AibB, that are independently required for AI-2 perception. AibA and AibB are conserved at greater than 95% identity at the amino acid sequence level throughout *H. pylori* species. Protein sequence homology identifies AibA as homologous to dipeptide binding proteins (39% identity with the *E. coli*

dipeptide binding protein; PDB identifier [ID] 1DPP) and AibB as homologous to molybdate binding proteins (36% identity to *Azotobacter vinelandii* periplasmic molybdate binding protein; PDB ID 1ATG). However, to our knowledge, this study was the first to demonstrate a function for these proteins. Despite the shared function of AI-2 binding, AibA, AibB, LsrB, and LuxP show little conservation in their amino acid sequences (see Fig. S8 in the supplemental material). We speculate that other bacteria may also have chemotactic responses to AI-2 that have not yet been identified due to the lack of sequence homology among AI-2 binding proteins.

The requirement of two PBPs for AI-2 perception is novel for chemotransduction and uncommon in signal transduction in general. In *Pseudomonas aeruginosa*, the FpvCDEF system for iron uptake requires two PBPs, FpvC and FpvF. However, in that system, a FpvC/FpvF complex is required for binding to ferric compounds (49). In contrast, AibA and AibB bind AI-2 independently *in vitro* (Fig. 2B). We do not yet know if AibA and AibB form a complex in the cell and, if so, in what stoichiometries, but this is a possible model for the chemorepellant response in *H. pylori* that we plan to explore in future work.

Responses to AI-2 on different time scales promote biofilm dispersal. Cell dispersal from biofilms is an important part of the life cycle of these structures. Although cells in biofilms benefit from protection from environmental stressors, a sedentary lifestyle is not always advantageous. It may be beneficial for cells to leave the biofilm if there are abundant external resources available or if resources are depleted at the biofilm site. The dispersal of cells from biofilms in response to chemical cues can be described as "bet hedging," which is an evolutionary response to changes in environments (50). When the chemical cue driving dispersal is endogenously produced and proportional to cell density, this provides a mechanism to maximize the ability of a population to explore new habitats and avoid depleting resources at the original site.

Cells can promote their dispersal from biofilms via several mechanisms that involve processes occurring over different time scales. A common mechanism for dispersal involves the downregulation of matrix-producing proteins and the upregulation of enzymes (proteases, DNases, etc.) to degrade the extracellular polymeric substances and nucleic acids that form the adherent matrix between cells of the biofilm (51, 52). Several bacterial species upregulate motility-associated genes, such as those required for flagellar biosynthesis, at the onset of dispersal (52). However, these mechanisms require changes in gene expression that take place over time scales of minutes to hours. A mechanism for more-rapid dispersal from biofilms is known as seeding dispersal, which has been shown to contribute to the virulence of several bacterial pathogens. Biofilms of *Pseudomonas aeruginosa*, *Staphylococcus aureus*, and other bacterial species (52) form hollow cavities containing nonadherent, motile cells. Upon the weakening of the extracellular matrix, these planktonic cells exit the biofilm in large numbers. Our work has shown that chemotactic responses, which occur on time scales of seconds to minutes, also provide a rapid mechanism for bacteria to exit a biofilm and would allow the structure to be much more plastic and adaptable to rapid fluctuations in the external or internal environment of the biofilm. It is likely that cells use multiple mechanisms of dispersal to orchestrate their exit from the biofilm when it is most advantageous to do so.

The spatial patterning of chemical cues can influence biofilm formation. *H. pylori* cells encounter a diversity of host- and microbe-derived signals in their native environment of the human stomach, and the integration of those signals determines the spatial distribution of the cells. Our experiments demonstrate that AI-2 chemotactic responses are necessary and sufficient for modulating *H. pylori* biofilm formation. We observed similar requirements for AI-2 production and reception for biofilms grown on glass frit or for microcolonies grown on epithelial cells. However, we noted that the chemotaxis-deficient *cheA* and *cheW* strains were less able to attach to or grow well on the MDCK cells. Previous work has shown that *H. pylori* uses chemotaxis as a guide to interact with the mouse stomach epithelium (53). We hypothesize that, in our system, epithelial cells provide *H. pylori* with more attractive cues than glass frit and thus that chemoattraction would play a more important role in the seeding of microcolonies on the epithelial surface than in the glass frit biofilm assay. Thus, in the case of growth on epithelial cells, the loss of chemotaxis would eliminate both attractive and repulsive drivers of microcolony formation, whereas on the glass frit only repulsive responses would be lost. This may explain the greater adherence of the chemotaxis-deficient mutant on the abiotic surface than on the biotic surface. The ΔaibA and ΔaibB strains, like the ΔcheA and ΔcheW strains, were unable to grow on the MDCK epithelial surface, in contrast to the ΔtlpB strain. We speculate that AibA and AibB function in processes other than AI-2 chemorepulsion (possibly chemotactic responses or transport of specific molecules) that render the mutant strains unable to attach to or grow on the MDCK cells.

Our results also provide insights into the spatial patterning of AI-2 during biofilm formation. We observed that adding exogenous AI-2 to a wild-type culture and a ΔluxS culture was sufficient to decrease the proportion of adherent cells in biofilms; however, this exogenous AI-2 addition to the ΔluxS culture could not return the proportional adherence to fully wild-type levels. We assume that the bulk addition of AI-2 at a single time point does not accurately recapitulate the concentrations and spatial distributions of endogenously produced AI-2 experienced by cells in the growing biofilm. Indeed, we observed stronger effects on biofilm structures by genetically manipulating the cells to overproduce AI-2 than by adding the chemical exogenously. We suggest that small or stochastic changes in the AI-2 environment during biofilm growth can alter the overall structure of the biofilm as it grows.

A striking effect of the loss of AI-2 production or sensing was the more homogenous spatial organization of the cells in the glass slide-grown biofilms, which appeared to be uniformly dispersed rather than heterogeneous clumps interspersed with sparse areas. We hypothesize that local fluctuations in AI-2 concentrations are important determinants of the spatial heterogeneities that are characteristic of wild-type *H. pylori* biofilms. One could even imagine a positive-feedback loop in which stochastic fluctuations in AI-2 concentrations would give rise to different local dispersal frequencies, creating heterogeneities in cell density that would enhance local variations in AI-2 concentrations. Interestingly, previous studies have shown that *luxS* expression in sessile biofilm populations is high for the first 2 days but decreases significantly in the biofilm cells after this time point (54, 55). Consistent with these observations, we observed a decrease in AI-2 concentrations in our glass frit biofilm assay over the course of 2 days (see Fig. S3D in the supplemental material). Such a downregulation of *luxS*

could mark a transition to a more mature biofilm stage with less cell dispersal. The spatial heterogeneities observed in our wild-type *H. pylori* biofilms resemble those described in other biofilm systems to be critical for nutrient and waste product flux and the overall fitness of the organisms within the biofilm structure (19). We speculate that because AI-2 chemorepulsion can operate on a short time scale and is sensitive to subtle spatial and temporal fluctuations in AI-2 concentrations, it serves as an important mechanism for generating the spatially heterogenous distribution of cells in a mature biofilm.

Chemotactic responses to quorum-sensing molecules as determinants of multispecies biofilm organization. The dynamics of biofilm formation and maturation requires complex, sequential mechanisms that give rise to an architectural structure that allows protection from environmental stressors, adequate nutrient and waste flow, and contact for bacteria with other cells and their host (56). We have shown that for *H. pylori* monospecies biofilm formation, chemorepulsion from AI-2 is a determinant of spatial organization and dispersal. Given that AI-2 is an important interspecies signaling molecule, we hypothesize that it may play an important role in mixed-species biofilm formation as well.

In addition to *H. pylori*, *E. coli* has also been shown to exhibit chemoresponses to AI-2, in this case sensing the quorum signal as a chemoattractant (21). Interestingly, biofilms of a Δ*luxS* strain of *E. coli* were found to be thinner and less dense than those of their wild-type counterparts (57), consistent with the absence of a self-produced attractant. Furthermore, the same study showed that the addition of exogenous AI-2 to Δ*luxS E. coli* biofilms resulted in a partial but significant rescue of biofilm biomass similar to the partial rescue we observed upon AI-2 addition to Δ*luxS H. pylori*. This suggests that AI-2 may influence spatial organization and adhesion in *E. coli* biofilms in a manner analogous to but opposite of that seen in *H. pylori* biofilms. *E. coli*'s ecological strategy may be to use AI-2 to localize and persist in the densely colonized colon, whereas *H. pylori* may use AI-2 to promote dispersal from individual gastric glands, where concentrations of AI-2 are likely to be high. Similarly to our observations with *H. pylori*, a *luxS* mutant of *Vibrio cholerae* was reported to develop more-adherent biofilms (58), implying a possible chemorepulsion response to AI-2.

Given that nearly all biofilms in nature are comprised of many organisms (3), it is interesting to speculate how collective AI-2 production and individual AI-2 perception could organize biofilm structures. High-AI-2 producers would serve as foci for those species attracted to AI-2, whereas AI-2 consumers could create permissive microenvironments for organisms averse to high AI-2 concentrations, with organisms with similar AI-2 preferences becoming segregated in the process. More generally, differential chemoresponses to bacterium-produced chemicals could be strong drivers of multispecies biofilm organization, layered upon the existing chemical landscape of the precolonized environment, be it a host tissue or an abiotic surface.

If AI-2 is a common chemotactic cue among bacteria, this knowledge could be harnessed for treatment of human infections. A recent report showed that AI-2 production by a colonic commensal, *Ruminococcus obeum*, can promote the resolution of *Vibrio cholerae* infection in a gnotobiotic mouse model, through an unknown mechanism (59). We speculate that commensals producing AI-2 at high levels may serve as sources of repulsive cues that drive *Vibrio cholerae* from the intestine. In the case of *H. pylori*, broad spread inflammation of gastric tissue throughout the organ is correlated with increased gastric cancer risk (60), presumably due to broader distribution of *H. pylori* bacteria in the stomach. It may be possible to manage the spread of *H. pylori* infection by inhibiting the AI-2 chemotaxis pathway to prevent dispersal of the cells to other areas of the stomach, thus reducing the risk for more-severe disease.

MATERIALS AND METHODS

***H. pylori* strains and bacterial culture.** *H. pylori* strain G27 was the primary strain used in this study (61), and it was the wild-type strain from which isogenic mutants were derived. Strains were grown on BBL and Columbia agar (BD) plates supplemented with 5% defibrinated horse blood, vancomycin (10 µg/µl), amphotericin B (8 µg/ml), and beta cyclodextrin (0.2% [wt/vol]) or in liquid brucella broth containing 10% fetal bovine serum (BB10) media under standard conditions, as previously described (45). Mutant strains were generated by PCR amplification of the appropriate antibiotic resistance gene, which was then incorporated via overlap extension PCR into a larger amplicon containing flanking sequences from the target gene (see Table S1 in the supplemental material). These PCR amplicons were introduced into G27 by natural transformation, and mutants in which the endogenous gene was disrupted by the insertion of the antibiotic resistance gene were selected using the appropriate antibiotic media and verified by PCR genotyping. Genetic complementation of disrupted genes was achieved by inserting the full coding region plus the predicted promoter sequence of the disrupted gene into the *rdxA* locus (62). The *aibA* complemention strain (*aibA**) replaced the wild-type gene at the endogenous locus with a copy of the *aibA* gene at the *rdxA* locus. Due to *aibA* being in a potential operon, the *aibB* promoter was inserted upstream of the *aibA* gene. The *aibB* complementation strain (*aibB**) replaced the wild-type gene at the endogenous locus with a copy of the *aibB* gene with the native putative promoter at the *rdxA* locus. The *luxS* overproducer strain (*luxS^{OP}*) was constructed by inserting an additional copy of *luxS* into the *rdxA* locus.

The *H. pylori* G27MA strain was used (46) for the microcolony experiments whose results are shown in Fig. 5 due to poor colonization by G27 on MDCK cell epithelia. Δ*cheW*, Δ*luxS*, and Δ*tlpB* mutants in strain G27MA were constructed by deletion of the *cheW*, *luxS*, and *tlpB* coding DNA sequences, respectively, using a PCR-based method as previously described (63). The coding DNA sequence of *cheW* and that of *luxS* were replaced with the APhA-encoding gene sequence (conferring kanamycin resistance). The coding DNA sequence of *tlpB* was replaced with the *cat* gene sequence (conferring chloramphenicol resistance). Mutants were selected on the appropriate antibiotic media and verified by PCR. Construction of Δ*cheA*, Δ*aibA*, and Δ*aibB* mutants in G27MA was achieved by isolation of genomic DNA from the respective G27 mutant strains and transformation into WT G27MA cultures. Mutants were selected by successful growth on kanamycin plates and were sequence verified.

Biofilm imaging. *H. pylori* cultures were grown in BB10 broth with shaking at 10% CO_2 at 37°C until an optical density at 600 nm (OD_{600}) of 0.6 to 0.9 was reached. The cultures were rediluted to 1×10^7 cells·ml^{-1}. One hundred microliters of culture was placed onto a clean glass slide (22 mm by 22 mm) and allowed to incubate in a humidified chamber for 5 days at 37°C and 10% CO_2, at which point a thick biofilm was readily visible on the air-liquid interface over the surface of the drop. The slides were carefully removed from the incubator and placed onto a 55°C heating block to gently evaporate the media, allowing the biofilm to settle onto the glass slide. The biofilm was fixed with 4% paraformaldehyde (PFA)–1× phosphate-buffered saline (PBS) for 15 min and then washed 3 times with 1× PBS. To visualize the results, one drop of Vectashield hard set with DAPI (Vector Labs) was added to the biofilm and the slide was covered with a coverslip. Biofilms were imaged with a 10× lens objective on a Nikon Eclipse TE2000-U microscope.

Frac-Lac analysis of biofilm images. For each slide, a minimum of three images were taken across the entirety of the biofilm. The contrast of

the biofilm images was altered in MatLab using the built-in function adapthisteq.m (contrast-limited adaptive histogram equalization [CLAHE]) with a ClipLimit parameter of 0.05. The altered images were thresholded using Otsu's method (see examples in Fig. S2A′ and B′ in the supplemental material). The resulting binary images were run through the FracLac plug-in in ImageJ (36, 64) to determine lacunarity with a Box Count analysis of binary images (black background) using a block series with 12 orientation positions and block sizes from 0 pixels to 32% of the image. Lacunarity scores were pooled by strain across a minimum of two experiments per strain.

Biofilm adherence assay. We used a biofilm adhesion assay that was previously described (24). *H. pylori* cultures were grown in BB10 to an OD_{600} of 0.6 to 0.9, and cultures were rediluted to 5×10^7 cells·ml^{-1}. Cultures (1 ml) were added to 12-well suspension culture plates (Olympus Plastics) filled approximately one-third full with autoclaved glass frit (Bullseye Glass) to increase the surface area available for cell attachment. Each experiment used 3 or 4 replicate wells filled with the same culture of *H. pylori*. The culture plates were incubated stationary for 2 days at 37°C and 10% CO_2, after which a biofilm at the air-liquid interface was observed. To quantify cells in the planktonic and biofilm populations, 1 ml of 1% crystal violet dye was added to cultures and allowed to incubate for 15 min. The liquid was removed via careful aspiration, and cells were spun down for 3 min at 13,500 rpm and saved as nonadherent cells. The adherent cells that were attached to the sides of the well and the frit were washed three times with 1 ml of 1× PBS. Each wash volume was added to the tube of nonadherent cells, spun down, and saved. After washes, the crystal violet in the cells of both the adherent and the nonadherent populations was extracted in 1 ml of 95% ethanol and the cells were pelleted by spinning at 13,500 rpm. The absorbance of the supernatant was then measured using a spectrophotometer at OD_{595}. Percent adherence of biofilm cells in the total population of the well was calculated as the absorbance of the adherent population divided by the sum of the absorbances of both the adherent and nonadherent cells, multiplied by 100.

For experiments adding exogenous AI-2 [(S)-4,5-dihydroxy-2,3-pentandione (DPD); Omm Scientific], strains were grown as described above. The culture was then split into two subcultures, one with AI-2 added to a final concentration of 37 nM and the other treated with an equal volume of BB10 as a control. The cultures were added to the glass frit and incubated for 2 days and analyzed as described above. The fraction of adherence of cultures with AI-2 addition was compared directly to the control results and was calculated by dividing the average percentage of cells in the biofilm of the AI-2-treated cultures by the average percentage of cells in the biofilm of the nontreated control.

For experiments where AI-2 was added to replacement media, the strains were grown as described above. After 48 h, the liquid medium was removed by pipette from each well. To wash the biofilm cells, 1 ml of BB10 was gently added to each well and removed. One milliliter of media, with or without the addition of AI-2 to achieve a final concentration of 37 nM, was added back to the wells, and the mixture was incubated for 24 h. The crystal violet assay was used to quantify the proportion of cells in the biofilm separately from the proportion of cells in the planktonic media. The change in biofilm mass or planktonic cell number after addition of AI-2 was calculated by finding the difference between the OD_{595} of cultures with AI-2 and the OD_{595} of the BB10 control.

Identification of putative periplasmic binding proteins in *H. pylori* G27. Proteins annotated as being "transport and binding proteins" in *H. pylori* strain J99 were identified using the resources of The Institute for Genomic Research (TIGR; J. Craig Venter Institute). The seven proteins were analyzed using the Basic Local Alignment Search Tool for proteins (BLASTp) for homology to other known periplasmic binding proteins. Of the seven, five protein candidates remained. The corresponding proteins and genes in *H. pylori* G27 were identified using BLASTp and were further characterized for roles in AI-2 chemotaxis.

Chemotaxis response assay. As previously described (22), *H. pylori* bacteria were inoculated into liquid BB10 media from plates and grown with shaking to an OD_{600} of 0.7 to 0.9. Cultures chosen for assay had at least 60% motile cells and minimal clumping. An 8-μl sample was spotted onto a glass slide and covered with a coverslip (22 mm by 22 mm). The coverslip was sealed on 3 sides with clear nail polish. Eight microliters of treatment (BB10, 100 mM HCl–BB10, or 100 μM synthetic AI-2–BB10) was added to the side of coverslip that was not sealed. After approximately 5 to 10 min, the culture was imaged at a magnification of ×10 through a 40× phase filter on a Leica DMIL microscope. The formation of a barrier indicated a response to treatment. Representative images were taken of the barrier or in similar locations on the slide under conditions with no barrier formation.

Protein purification and AI-2 binding assay. Assessments of the AI-2 binding ability of proteins were based on previous methods (41, 42). LsrB (kindly provided by Stephen T. Miller, Swarthmore College, Swarthmore, PA) was cloned into the pGex-4T-1 expression vector. The periplasmic portion of the *tlpB* gene (coding for TlpB residues 33 to 211) was cloned into a pGex-4T-1 expression vector. The *aibA* and *aibB* genes lacking the periplasmic targeting sequence (*aibA* lacking the coding region for amino acids 1 to 22, *aibB* lacking the coding region for amino acids 1 to 24) were cloned into a pGex-6P-1 expression vector (GE Healthcare). The plasmids were transformed into BL21 *E. coli* for protein expression. Protein purification was achieved using a glutathione Sepharose 4B column (GE Healthcare) following the recommended protocol. The glutathione S-transferase (GST) tag was left on the purified proteins after we determined that GST alone did not show AI-2 binding activity (data not shown). The GST tag was cleaved from AibB because of apparent partial spontaneous cleavage of the GST tag during purification. GST cleavage was achieved after elution of AibB from the column by adding 1 unit of PreScission protease enzyme and incubation overnight at 4°C per the instructions of the manufacturer (GE Healthcare). Purified proteins were dialyzed into a storage buffer consisting of 300 mM NaCl, 10 μM Tris (pH 8), and 5 μM 2-mercaptoethanol, concentrated with a VivaSpin-20 filter (GE Healthcare), and stored at −80°C.

For the protein–AI-2 binding assay, all purified proteins were normalized by dilution into assay buffer (300 mM NaCl, 10 mM sodium phosphate, pH 7) to a concentration of 6 mg ml^{-1} as quantified by the use of a NanoDrop-1000 spectrophotometer (Thermo-Fisher Scientific). Protein (200 μl) was incubated with 100 μl of 1 mM synthetic AI-2 diluted into assay buffer at 4°C for 120 min. The sample was loaded onto a Sepharose G_{25} fine column (Sigma Aldrich). The column was washed with 4 200-μl volumes of assay buffer, and the eluate was collected. The eluted protein was quantified by direct application of the sample to the NanoDrop spectrophotometer and concentrated to 100 μl using an Amicon Ultra 10-K membrane centrifugal filter. Retentate was incubated in a 55°C water bath for 10 min to denature the protein and release any bound AI-2 into the supernatant. The sample was centrifuged at 14,000 rpm for 2 min to pellet protein.

The supernatant was directly used in a *Vibrio harveyi* luminescence assay to test for AI-2 levels as previously described (45). Briefly, an overnight culture of *V. harveyi* was diluted 1:5,000 in fresh AB medium (300 mM NaCl, 50 mM $MgSO_4$, 2% [wt/vol] Casamino Acids, 10 mM potassium phosphate [pH 7], 1 mM L-arginine, 1% [wt/vol] glycerol). Ninety microliters of diluted *V. harveyi* culture was added to 10 μl of protein supernatant and put into a 96-well plate in triplicate experiments. Levels of luminescence were measured on a SpectraMax M5e plate reader (Molecular Devices) each hour over the course of 6 h with incubation on a shaker at 30°C between measurements. Levels of relative luminescence units (RLUs) for each sample were taken at the time point where there was the largest difference between an exogenous AI-2 positive control and a buffer negative control, and the data were normalized as a percentage of the exogenous AI-2 positive control data.

Cell culture. Madin-Darby canine kidney II (MDCK) cells (kindly provided by W. James Nelson, Stanford, CA) (65) were grown in Dulbecco's modified Eagle's medium (DMEM) (Gibco) containing 10% fetal bovine serum (FBS) (Gibco) at 37°C in a 5% CO_2 atmosphere. Polarized

MDCK monolayers were generated as previously described (25). Briefly, about a half-million cells were seeded onto 12-mm-diameter, 0.4-μm-pore-size polycarbonate tissue culture insertions (Transwell filters; Corning Costar). At 1 day after seeding, the apical medium was changed to DMEM and the basal medium was changed to DMEM–10% FBS. For four subsequent days, the basal medium was replaced daily with fresh DMEM–10% FBS whereas the apical medium was unchanged. On the fifth day postseeding, the monolayers were ready for use.

H. *pylori* infection of polarized MDCK monolayers. The basal media of polarized monolayers were replaced with coculture medium (DMEM–10% FBS–10% *Brucella* broth). The apical surfaces of polarized monolayers were washed 3 times with DMEM. Then, 500 μl of a bacterial culture at an OD_{600} of 0.2 (~10^8 CFU/ml) was added to the apical side of the monolayer and allowed to infect the monolayer for 5 min at 37°C in a 5% CO_2 atmosphere. Infected monolayers were washed 4 times with fresh DMEM to remove nonadherent bacteria. DMEM was added back to the apical side of the monolayer, and the cells were kept at 37°C in a 5% CO_2 atmosphere. Each day for 3 days, the basal medium was replaced with fresh coculture medium, the apical chamber was sampled for CFU levels, and the monolayers were washed 4 times with DMEM before fresh DMEM was added back.

Confocal immunofluorescence microscopy and antibodies. At terminal time points, samples were fixed and processed for confocal immunofluorescence as previously described (66). Chicken anti-*H. pylori* G27MA (46) was used at a 1:500 dilution, and mouse anti-ZO-1 was used at 1:100. *H. pylori* was detected using a goat anti-chicken 594 secondary antibody, and ZO-1 was detected using a goat anti-mouse 488 secondary antibody. DAPI (Invitrogen) was also used to stain for cell nuclei. Samples were imaged at a magnification of ×40 with a Zeiss LSM 700 confocal microscope, and extended-focus images of z-stacks were analyzed via a custom MatLab script.

Measuring AI-2 production in H. *pylori*. WT, *luxS*^{OP}, and Δ*luxS* *H. pylori* cultures were inoculated into 3 ml BB10 from plates. Four hours after inoculation, cultures were diluted back to 5×10^7 cells ml^{-1} and incubated with shaking at 37°C and 10% CO_2. Samples of WT and *luxS*^{OP} cultures were taken at 4, 8, 12, 24, 36, and 48 h postdilution and analyzed for optical density and CFU levels on plates. Samples of WT, *luxS*^{OP}, and Δ*luxS* cells were taken at each time point and spun down at 13,500 rpm for 3 min, and the cell-free supernatant (CFS) was saved and stored at −20°C. The CFS was analyzed for AI-2 using the *Vibrio harveyi* luminescence assay. Ten microliters of CFS was added to 90 μl of *V. harveyi* culture (prepared as previously described for the AI-2 binding assay) with duplicate samples in a 96-well plate. Levels of luminescence were measured on a SpectraMax M5e plate reader (Molecular Devices) each hour over the course of 6 h with incubation on a shaker at 30°C between measurements. Levels of relative luminescence units (RLUs) were taken at the time point where there was the largest difference between an exogenous DPD positive control and the Δ*luxS* negative control.

cDNA synthesis. WT, Δ*aibA*, *aibA**, Δ*aibB*, *aibB**, Δ*tlpB*, and *tlpB*^{D114N} strains were inoculated into liquid BB10 media from plates and grown with shaking to an OD_{600} of 1. Cultures were spun at 4,000 rpm to pellet cells and resuspended in 700 μl of TRIzol reagent (Life Technologies). RNA was extracted following the TRIzol sample preparation protocol provided by the manufacturer, and the RNA pellet was resuspended in RNase-free water. The RNA was treated with DNase-1 (New England Biolabs) to degrade contaminant genomic DNA following the manufacturer's protocol. A 5-μg volume of RNA, 50 ng/μl random hexamer primers, and SuperScript III reverse transcriptase (Life Technologies) were used to generate cDNA following the manufacturer's protocol. The resulting cDNA was treated with RNase H (Life Technologies) to degrade template RNA.

qRT-PCR. Synthesized cDNA was amplified using primers targeting ~100-bp sequences of *aibA*, *aibB*, and *tlpB* genes, with *ureA* and *ureB* targets as endogenous controls. Primer efficiency was confirmed to be >95% for each primer set used. qRT-PCR reaction mixtures contained 5 μl Kapa SYBR Fast quantitative PCR (qPCR) master mix (Kapa Biosystems), 1 μl cDNA, and 10 μM (each) forward and reverse primers, and water was added to achieve a 10-μl reaction volume. Standard qRT-PCR reactions were performed in experimental triplicates on an Applied Biosystems StepOnePlus PCR machine (Life Technologies) and analyzed using StepOne software (version 2.2.2) to calculate the quantity of target cDNA in mutant and complement strains relative to the WT level using both *ureA* and *ureB* as endogenous controls.

Protein sequence alignment. Gene and protein sequences for *H. pylori* G27 AibA (HPG27_277; *hbpA*) and AibB (HPG27_431; *modA*) were acquired from the University of California, Santa Cruz (UCSC) Microbial Genome Browser (67). Representative LuxP (*Vibrio cholera*; GenBank accession no. KFE33015.1) and LsrB (*Escherichia coli* 101-1; GenBank accession no. EDX40441.1) sequences were aligned with the AibA and AibB sequences using ClustalW2 multiple-protein sequence alignment (EMBL-EBI).

Statistical analysis. All data analysis was performed using R (68) unless otherwise specified. A *P* value of 0.05 was used as a cutoff to determine significance. All experiments had a minimum of 3 replicates unless otherwise specified.

For data analysis of biofilm lacunarity (Fig. 1F and 3H), statistical analysis was performed in GraphPad Prism (version 6.03 for Windows; GraphPad Software, San Diego, CA, USA) by pooling the lacunarity scores of individual images from different experiments and comparing the pooled scores to the WT scores using Student's *t* test. For determinations of percentages of cells in biofilm (Fig. 1H and 3I), percentages of cells in biofilm from multiple experiments were pooled, transformed using arcsine square root calculations, and assessed with one-way analysis of variance (ANOVA) and Tukey's honestly significant difference (HSD) test against the WT data. To determine the significance of increased RLUs (Fig. 2B), the percentages of RLUs from replicate experiments were pooled and compared to the buffer negative-control value using Student's *t* test to determine significance. For analysis of the changes seen with AI-2 addition (Fig. 4A), the differences in the percentages of cells in biofilm for each experiment were pooled and tested against the null hypothesis of a μ value of 0 (no change) using Student's *t* test. For analysis of the changes of the fractions seen with AI-2 addition to replacement media (Fig. 4B), the values were pooled from multiple experiments and tested against the null hypothesis of a μ value of 1 (no change) using Student's *t* test. To calculate the estimated number of attached bacteria on MDCK cells (Fig. 5D), the images of *H. pylori* microcolony cells were quantified using MatLab to measure the size of microcolonies in pixels. The value for the most populous bin of pixel intensity distribution of cells after 5 min of attachment, in which state most bacteria are present as single cells, was 20 pixels. The number of cells in the microcolonies was estimated by dividing the number of pixels in the microcolony by 20. The number of *H. pylori* cells in the field of view was extrapolated to estimate the number of attached *H. pylori* cells in the entire transwell, and the results determined among the triplicate fields of view taken in the same well were averaged. Analysis of the significance of the differences between the results determined for 3 days of attachment and those determined for 5 min of attachment within strains was achieved by performing Student's *t* test using GraphPad Prism. To compare average microcolony sizes (Fig. 5E), the averages of the microcolony sizes at 3 days were pooled and compared to the WT data with one-way analysis of variance and Tukey's test using GraphPad Prism. For comparing growth rates (see Fig. S1A in the supplemental material) and RLU data (see Fig. S1B), the duplicate values for *lux*^{OP} in each experiment were pooled and compared to WT values using Student's *t* test.

SUPPLEMENTAL MATERIAL

Supplemental material for this article may be found at http://mbio.asm.org/lookup/suppl/doi:10.1128/mBio.00379-15/-/DCSupplemental.

Figure S1, EPS file, 0.3 MB.
Figure S2, TIF file, 0.7 MB.
Figure S3, EPS file, 0.4 MB.
Figure S4, EPS file, 1.2 MB.

Figure S5, EPS file, 0.1 MB.
Figure S6, EPS file, 0.1 MB.
Figure S7, EPS file, 1.6 MB.
Figure S8, EPS file, 0.1 MB.
Table S1, EPS file, 0.2 MB.

REFERENCES

1. **Wozniak DJ, Parsek MR**. 2014. Surface-associated microbes continue to surprise us in their sophisticated strategies for assembling biofilm communities. F1000PrimeRep **6**:26. http://dx.doi.org/10.12703/P6-26.
2. **De la Fuente-Núñez C, Reffuveille F, Fernández L, Hancock RE**. 2013. Bacterial biofilm development as a multicellular adaptation: antibiotic resistance and new therapeutic strategies. Curr Opin Microbiol **16**:580–589. http://dx.doi.org/10.1016/j.mib.2013.06.013.
3. **Elias S, Banin E**. 2012. Multi-species biofilms: living with friendly neighbors. FEMS Microbiol Rev **36**:990–1004. http://dx.doi.org/10.1111/j.1574-6976.2012.00325.x.
4. **Donlan RM**. 2002. Biofilms: microbial life on surfaces. Emerg Infect Dis **8**:881–890. http://dx.doi.org/10.3201/eid0809.020063.
5. **Davey ME, George AO**. 2000. Microbial biofilms: from ecology to molecular genetics. Microbiol Mol Biol Rev **64**:847–867. http://dx.doi.org/10.1128/MMBR.64.4.847-867.2000.
6. **Kostakioti M, Hadjifrangiskou M, Hultgren SJ**. 2013. Bacterial biofilms: development, dispersal, and therapeutic strategies in the dawn of the post-antibiotic era. Cold Spring Harb Perspect Med **3**:a010306. http://dx.doi.org/10.1101/cshperspect.a010306.
7. **Flemming H-C, Wingender J**. 2010. The biofilm matrix. Nat Rev Microbiol **8**:623–633. http://dx.doi.org/10.1038/nrmicro2415.
8. **Moreau-Marquis S, Stanton BA, O'Toole GA**. 2008. Pseudomonas aeruginosa biofilm formation in the cystic fibrosis airway. Pulm Pharmacol Ther **21**:595–599. http://dx.doi.org/10.1016/j.pupt.2007.12.001.
9. **Kaplan JB**. 2010. Biofilm dispersal: mechanisms, clinical implications, and potential therapeutic uses. Crit Rev Oral Biol Med **89**:205–218. http://dx.doi.org/10.1177/0022034509359403.
10. **Hall-Stoodley L, Stoodley P**. 2005. Biofilm formation and dispersal and the transmission of human pathogens. Trends Microbiol **13**:7–10. http://dx.doi.org/10.1016/j.tim.2004.11.004.
11. **Rutherford ST, Bassler BL**. 2012. Bacterial quorum sensing: its role in virulence and possibilities for its control. Cold Spring Harb Perspect Med **2**:a012427. http://dx.doi.org/10.1101/cshperspect.a012427.
12. **Li Y-H, Tian X**. 2012. Quorum sensing and bacterial social interactions in biofilms. Sensors (Basel) **12**:2519–2538. http://dx.doi.org/10.3390/s120302519.
13. **González JE, Keshavan ND**. 2006. Messing with bacterial quorum sensing. Microbiol Mol Biol Rev **70**:859–875. http://dx.doi.org/10.1128/MMBR.00002-06.
14. **Marketon MM, Glenn SA, Eberhard A, González JE**. 2003. Quorum sensing controls exopolysaccharide production in Sinorhizobium meliloti. J Bacteriol **185**:325–331. http://dx.doi.org/10.1128/JB.185.1.325-331.2003.
15. **Parsek MR, Greenberg EP**. 1999. Quorum sensing signals in development of Pseudomonas aeruginosa biofilms. Methods Enzymol **310**:43–55.
16. **Spoering AL, Gilmore MS**. 2006. Quorum sensing and DNA release in bacterial biofilms. Curr Opin Microbiol **9**:133–137. http://dx.doi.org/10.1016/j.mib.2006.02.004.
17. **Boles BR, Horswill AR**. 2008. Agr-mediated dispersal of Staphylococcus aureus biofilms. PLoS Pathog **4**:e1000052. http://dx.doi.org/10.1371/journal.ppat.1000052.
18. **Claessen D, Rozen DE, Kuipers OP, Søgaard-Andersen L, van Wezel GP**. 2014. Bacterial solutions to multicellularity: a tale of biofilms, filaments and fruiting bodies. Nat Rev Microbiol **12**:115–124. http://dx.doi.org/10.1038/nrmicro3178.
19. **Monds RD, O'Toole GA**. 2009. The developmental model of microbial biofilms: ten years of a paradigm up for review. Trends Microbiol **17**:73–87. http://dx.doi.org/10.1016/j.tim.2008.11.001.
20. **Kaiser D**. 2003. Coupling cell movement to multicellular development in myxobacteria. Nat Rev Microbiol **1**:45–54. http://dx.doi.org/10.1038/nrmicro733.
21. **Hegde M, Englert DL, Schrock S, Cohn WB, Vogt C, Wood TK, Manson MD, Jayaraman A**. 2011. Chemotaxis to the quorum-sensing signal AI-2 requires the Tsr chemoreceptor and the periplasmic LsrB AI-2-binding protein. J Bacteriol **193**:768–773. http://dx.doi.org/10.1128/JB.01196-10.
22. **Rader BA, Wreden C, Hicks KG, Sweeney EG, Ottemann KM, Guillemin K**. 2011. Helicobacter pylori perceives the quorum-sensing molecule AI-2 as a chemorepellent via the chemoreceptor TlpB. Microbiology **157**:2445–2455. http://dx.doi.org/10.1099/mic.0.049353-0.
23. **Stark RM, Gerwig GJ, Pitman RS, Potts LF, Williams NA, Greenman J, Weinzweig IP, Hirst TR, Millar MR**. 1999. Biofilm formation by Helicobacter pylori. Lett Appl Microbiol **28**:121–126. http://dx.doi.org/10.1046/j.1365-2672.1999.00481.x.
24. **Cole SP, Harwood J, Lee R, She R, Guiney DG**. 2004. Characterization of monospecies biofilm formation by Helicobacter pylori. J Bacteriol **186**:3124–3132. http://dx.doi.org/10.1128/JB.186.10.3124-3132.2004.
25. **Tan S, Noto JM, Romero-Gallo J, Peek RM, Amieva MR**. 2011. Helicobacter pylori perturbs iron trafficking in the epithelium to grow on the cell surface. PLoS Pathog **7**:e1002050. http://dx.doi.org/10.1371/journal.ppat.1002050.
26. **Howitt MR, Lee JY, Lertsethtakarn P, Vogelmann R, Joubert LM, Ottemann KM, Amieva MR**. 2011. ChePep controls Helicobacter pylori infection of the gastric glands and chemotaxis in the Epsilonproteobacteria. mBio **2**:00098-11. http://dx.doi.org/10.1128/mBio.00098-11.
27. **Carron MA, Tran VR, Sugawa C, Coticchia JM**. 2006. Identification of Helicobacter pylori biofilms in human gastric mucosa. J Gastrointest Surg **10**:712–717. http://dx.doi.org/10.1016/j.gassur.2005.10.019.
28. **Coticchia JM, Sugawa C, Tran VR, Gurrola J, Kowalski E, Carron MA**. 2006. Presence and density of Helicobacter pylori biofilms in human gastric mucosa in patients with peptic ulcer disease. J Gastrointest Surg **10**:883–889. http://dx.doi.org/10.1016/j.gassur.2005.12.009.
29. **García A, Salas-Jara MJ, Herrera C, González C**. 2014. Biofilm and Helicobacter pylori: from environment to human host. World J Gastroenterol **20**:5632–5638. http://dx.doi.org/10.3748/wjg.v20.i19.5632.
30. **Sigal M, Rothenberg ME, Logan CY, Lee JY, Honaker RW, Cooper RL, Passarelli B, Camorlinga M, Bouley DM, Alvarez G, Nusse R, Torres J, Amieva MR**. 2015. Helicobacter pylori Activate and Expand Lgr5+ stem cells through direct colonization of the gastric glands. Gastroenterology **148**:1392–1404. e21. http://dx.doi.org/10.1053/j.gastro.2015.02.049.
31. **Mackay WG, Gribbon LT, Barer MR, Reid DC**. 1998. Biofilms in drinking water systems—a possible reservoir for Helicobacter pylori. Water Sci Technol **38**(Suppl 1):181–185. http://dx.doi.org/10.1111/j.1365-2672.1998.tb05283.x.
32. **Gião MS, Azevedo NF, Wilks SA, Vieira MJ, Keevil CW**. 2011. Interaction of Legionella pneumophila and Helicobacter pylori with bacterial species isolated from drinking water biofilms. BMC Microbiol **11**:57. http://dx.doi.org/10.1186/1471-2180-11-57.
33. **Cellini L**. 2014. Helicobacter pylori: a chameleon-like approach to life. World J Gastroenterol **20**:5575–5582. http://dx.doi.org/10.3748/wjg.v20.i19.5575.
34. **Grande R, Di Giulio M, Bessa LJ, Di Campli E, Baffoni M, Guarnieri S, Cellini L**. 2011. Extracellular DNA in Helicobacter pylori biofilm: a backstairs rumour. J Appl Microbiol **110**:490–498. http://dx.doi.org/10.1111/j.1365-2672.2010.04911.x.
35. **Gölz G, Sharbati S, Backert S, Alter T**. 2012. Quorum sensing dependent phenotypes and their molecular mechanisms in *Campylobacterales*. Eur J

Microbiol Immunol **2**:50–60. http://dx.doi.org/10.1556/EuJMI.2.2012.1.8.

36. **Karperien A**. 2013. FracLac for ImageJ. http://rsb.info.nih.gov/ij/plugins/fraclac/FLHelp/Introduction.htm.

37. **Tolle CR, McJunkin TR, Rohrbaugh DT, LaViolette RA**. 2003. Lacunarity definition for ramified data sets based on optimal cover. Phys D Nonlinear Phenom **179**:129–152. http://dx.doi.org/10.1016/S0167-2789(03)00029-0.

38. **Vendeville A, Winzer K, Heurlier K, Tang CM, Hardie KR**. 2005. Making "sense" of metabolism: autoinducer-2, LuxS and pathogenic bacteria. Nat Rev Microbiol **3**:383–396. http://dx.doi.org/10.1038/nrmicro1146.

39. **Altschul SF, Gish W, Miller W, Myers EW, Lipman DJ**. 1990. Basic local alignment search tool. J Mol Biol **215**:403–410. http://dx.doi.org/10.1016/S0022-2836(05)80360-2.

40. **Szurmant H, Ordal GW**. 2004. Diversity in chemotaxis mechanisms among the Bacteria and Archaea. Microbiol Mol Biol Rev **68**:301–319. http://dx.doi.org/10.1128/MMBR.68.2.301-319.2004.

41. **Miller ST, Xavier KB, Campagna SR, Taga ME, Semmelhack MF, Bassler BL, Hughson FM**. 2004. Salmonella typhimurium recognizes a chemically distinct form of the bacterial quorum-sensing signal AI-2. Mol Cell **15**:677–687. http://dx.doi.org/10.1016/j.molcel.2004.07.020.

42. **Chen X, Schauder S, Potier N, Van Dorsselaer A, Pelczer I, Bassler BL, Hughson FM**. 2002. Structural identification of a bacterial quorum-sensing signal containing boron. Nature **415**:545–549. http://dx.doi.org/10.1038/415545a.

43. **Zhu J, Pei D**. 2008. A LuxP-based fluorescent sensor for bacterial autoinducer II. ACS Chem Biol **3**:110–119. http://dx.doi.org/10.1021/cb7002048.

44. **Sweeney EG, Henderson JN, Goers J, Wreden C, Kevin G, Foster JK, Parthasarathy R, Remington SJ, Guillemin K**. 2012. Structure and proposed mechanism for the pH-sensing Helicobacter pylori chemoreceptor TlpB. Cell Struct **20**:1177–1188.

45. **Rader BA, Campagna SR, Semmelhack MF, Bassler BL, Guillemin K**. 2007. The quorum-sensing molecule autoinducer 2 regulates motility and flagellar morphogenesis in Helicobacter pylori. J Bacteriol **189**:6109–6117. http://dx.doi.org/10.1128/JB.00246-07.

46. **Amieva MR, Vogelmann R, Covacci A, Tompkins LS, Nelson J, Falkow S**. 2003. Disruption of the epithelial apical-junctional complex by Helicobacter pylori CagA-80. Science **300**:1430–1434.

47. **Neiditch MB, Federle MJ, Miller ST, Bassler BL, Hughson FM**. 2005. Regulation of LuxPQ receptor activity by the quorum-sensing signal autoinducer-2. Mol Cell **18**:507–518. http://dx.doi.org/10.1016/j.molcel.2005.04.020.

48. **Pereira CS, de Regt AK, Brito PH, Miller ST, Xavier KB**. 2009. Identification of functional LsrB-like autoinducer-2 receptors. J Bacteriol **191**:6975–6987. http://dx.doi.org/10.1128/JB.00976-09.

49. **Brillet K, Ruffenach F, Adams H, Journet L, Gasser V, Hoegy F, Guillon L, Hannauer M, Page A, Schalk IJ**. 2012. An ABC transporter with two periplasmic binding proteins involved in iron acquisition in Pseudomonas aeruginosa. ACS Chem Biol **7**:2036–2045. http://dx.doi.org/10.1021/cb300330v.

50. **McDougald D, Rice SA, Barraud N, Steinberg PD, Kjelleberg S**. 2012. Should we stay or should we go: mechanisms and ecological consequences for biofilm dispersal. Nat Rev Microbiol **10**:39–50. http://dx.doi.org/10.1038/nrmicro2695.

51. **Nijland R, Hall MJ, Burgess JG**. 2010. Dispersal of biofilms by secreted, matrix degrading, bacterial DNase. PLoS One **5**:e15668. http://dx.doi.org/10.1371/journal.pone.0015668.

52. **Kaplan JB**. 2009. Therapeutic potential of biofilm-dispersing enzymes. Int J Artif Organs **32**:545–554.

53. **Williams SM, Chen Y-T, Andermann TM, Carter JE, McGee DJ, Ottemann KM**. 2007. Helicobacter pylori chemotaxis modulates inflammation and bacterium-gastric epithelium interactions in infected mice. Infect Immun **75**:3747–3757. http://dx.doi.org/10.1128/IAI.00082-07.

54. **Cellini L, Grande R, Traini T, Di Campli E, Di Bartolomeo S, Di Iorio D, Caputi S**. 2005. Biofilm formation and modulation of luxS and rpoD expression by Helicobacter pylori. Biofilms **2**:119–127. http://dx.doi.org/10.1017/S1479050505001845.

55. **Cellini L, Grande R, Di Campli E, Di Bartolomeo S, Di Giulio M, Traini T, Trubiani O**. 2008. Characterization of an Helicobacter pylori environmental strain. J Appl Microbiol **105**:761–769. http://dx.doi.org/10.1111/j.1365-2672.2008.03808.x.

56. **Abee T, Kovács AT, Kuipers OP, van der Veen S**. 2011. Biofilm formation and dispersal in Gram-positive bacteria. Curr Opin Biotechnol **22**:172–179. http://dx.doi.org/10.1016/j.copbio.2010.10.016.

57. **Niu C, Robbins CM, Pittman KJ, Osborn JL, Stubblefield BA, Simmons RB, Gilbert ES**. 2013. LuxS influences Escherichia coli biofilm formation through autoinducer-2-dependent and autoinducer-2-independent modalities. FEMS Microbiol Ecol **83**:778–791. http://dx.doi.org/10.1111/1574-6941.12034.

58. **Ali SA, Benitez JA**. 2009. Differential response of Vibrio cholerae planktonic and biofilm cells to autoinducer 2 deficiency. Microbiol Immunol **53**:582–586. http://dx.doi.org/10.1111/j.1348-0421.2009.00161.x.

59. **Hsiao A, Ahmed AM, Subramanian S, Griffin NW, Drewry LL, Petri WA, Haque R, Ahmed T, Gordon JI**. 2014. Members of the human gut microbiota involved in recovery from Vibrio cholerae infection. Nature **515**:423–426. http://dx.doi.org/10.1038/nature13738.

60. **Amieva MR, El-Omar EM**. 2008. Host-bacterial interactions in Helicobacter pylori infection. Gastroenterology **134**:306–323. http://dx.doi.org/10.1053/j.gastro.2007.11.009.

61. **Covacci A, Censini S, Bugnoli M, Petracca R, Burroni D, Macchia G, Massone A, Papini E, Xiang Z, Figura N, Rappuoli R**. 1993. Molecular characterization of the 128-kDa immunodominant antigen of Helicobacter pylori associated with cytotoxicity and duodenal ulcer. Proc Natl Acad Sci U S A **90**:5791–5795. http://dx.doi.org/10.1073/pnas.90.12.5791.

62. **Smeets LC, Bijlsma JJ, Boomkens SY, Vandenbroucke-Grauls CM, Kusters JG**. 2000. comH, a novel gene essential for natural transformation of Helicobacter pylori. J Bacteriol **182**:3948–3954. http://dx.doi.org/10.1128/JB.182.14.3948-3954.2000.

63. **Chalker AF, Minehart HW, Hughes NJ, Koretke KK, Lonetto MA, Brinkman KK, Warren PV, Lupas A, Stanhope MJ, Brown JR, Hoffman PS**. 2001. Systematic identification of selective essential genes in Helicobacter pylori by genome prioritization and allelic replacement mutagenesis. J Bacteriol **183**:1259–1268.

64. **Rasband W**. 2012. ImageJ. U.S. National Institutes of Health, Bethesda, MD. http://imagej.nih.gov/ij.

65. **Tamada M, Perez TD, Nelson WJ, Sheetz MP**. 2007. Two distinct modes of myosin assembly and dynamics during epithelial wound closure. J Cell Biol **176**:27–33. http://dx.doi.org/10.1083/jcb.200609116.

66. **Pentecost M, Otto G, Theriot JA, Amieva MR**. 2006. Listeria monocytogenes invades the epithelial junctions at sites of cell extrusion. PLoS Pathog **2**:e3. http://dx.doi.org/10.1371/journal.ppat.0020003.

67. **Karolchik D, Baertsch R, Diekhans M, Furey TS, Hinrichs A, Lu YT, Roskin KM, Schwartz M, Sugnet CW, Thomas DJ, Weber RJ, Haussler D, Kent WJ, University of California Santa Cruz**. 2003. The UCSC Genome Browser Database. Nucleic Acids Res **31**:51–54. http://dx.doi.org/10.1093/nar/gkg129.

68. **R Development Core Team**. 2012. R: a language and environment for statistical computing. http://www.R-project.org/.